Analysis of a transverse combustion instability in a full rocket engine under supercritical conditions

By L. Selle †, A. Urbano ‡, Q. Douasbin †, T. Schmitt ¶ AND S. Ducruix ¶

Transverse combustion instabilities in rocket engines are a major risk, but fundamental knowledge of the physical mechanisms driving these instabilities is limited. The coaxial diffusion flames typically used in most liquid-propellant rocket engines are submitted to both pressure and transverse velocity fluctuations, yet it is still unclear how this forcing may drive or damp acoustic fluctuations. The present work uses a database of Large-Eddy Simulations (LES) under both stable and unstable conditions to quantify the interaction between acoustics and combustion. The configuration is a reduced-scale 42-injector rocket engine using hydrogen and oxygen as propellants and operating at supercritical pressure. As the LES exhibits a non-linearly unstable operating condition, a mechanism responsible for this triggering is proposed.

1. Introduction

Avoiding the occurrence of combustion instabilities (CI) is one of the most critical requirements in the development of high-performance combustion engines. Because only a minute fraction (as little as 10^{-4}) of the energy released by combustion is enough to provoke a destructive instability (Culick 1988), any engine will most likely be unstable –and dangerously close to failure– within a certain range of operating conditions. For example, the development of the F1 engine that brought man to the Moon during the Apollo program, required 1332 full-scale hot-fire tests and 108 injector design changes before meeting both stability and performance requirements (Anderson & Yang 1995; Oefelein & Yang 1993).

Combustion instabilities result from the constructive coupling between acoustic waves and unsteady heat release rate. There are essentially two conditions for CI to occur, namely

(a) The first one attributed to Rayleigh (1878), states that the integral over a period of the oscillation of the product of pressure (p') and heat release rate (q') fluctuations must be positive. This imposes a constraint on the phase (or the time delay) between p' and q'.

(b) The second condition is that the energy fed into acoustics by combustion must overcome the fluxes at the boundaries and the various internal losses (Lieuwen 2012, Ch. 6). Thus, the gain of the destabilizing process must exceed a certain threshold value (Poinsot & Veynante 2011, Ch. 8).

These criteria can be expressed in an accurate mathematical form by studying the conservation equation for acoustic energy, (cf. Section 4).

In predicting CI using low-order models, i.e., not solely from first principles, various

† Institut de Mécanique des Fluides de Toulouse (IMFT), France
‡ Safran, France
¶ École Centrale Paris, France

levels of approximation may be considered but depending on the physical or geometrical complexity considered, it comes down to the resolution of an algebraic or differential system where a model for the unsteady heat release rate q' is the missing information. For this purpose, the so called $n-\tau$ model initially proposed by Crocco (1951, 1952) relates q' to p' via a gain, n, and a time delay, τ. The formalisms of the Flame Transfer Function (FTF) or Flame Describing Function (FDF) have subsequently been refined many times, but the key idea nevertheless remains the same.

Unfortunately, it is almost impossible to determine the stability map and stability margins of an engine at the design stage with current tools. Guidelines for design and flight certification in the aerospace industry are still based on experimental knowledge dating back to the 1940's and 60's (Harrje & Reardon 1972). CI are usually classified according to the frequency of the oscillations. For instabilities below 100 Hz, the term chugging is common, while above several hundreds or thousands of cycles per second, names such as screaming or screeching are often used. While the low-frequency CI are relatively easy to avoid, high-frequency CI are much harder to mitigate, especially those with a structure transverse to the mean flow. It is therefore critical to understand what drives transverse modes. Sometimes, these transverse modes cannot be avoided even with proper design so that they must be damped by the addition of cavities (Searby *et al.* 2008) or baffles (Oefelein & Yang 1993; You *et al.* 2013) in the combustion chamber. There have been many attempts to predict transverse modes with low-order models, but lack of knowledge about the flame response limits these studies to parametric variations for n and τ (Crocco *et al.* 1962; Sirignano & Popov 2013; Popov *et al.* 2014). Understanding how flames respond to transverse excitation is a crucial research imperative. Indeed, for transverse modes, both pressure, axial and tangential velocity fluctuations may affect the flame, which would mean that three input variables may be necessary to model the flame response rather than only one as in the standard model of Crocco.

Some insight was gained by the experimental investigation of multiple-injector combustion chambers with optical access (Lubarsky *et al.* 2008; Méry *et al.* 2013; Hardi *et al.* 2014) but as these configurations have only a few injectors, it is often necessary to force acoustics externally because transverse CI do not occur naturally. With regard to numerical simulations, there have been some attempts to compute flame responses (Sattelmayer *et al.* 2015; Hakim *et al.* 2015) but, as explained by Sirignano & Popov (2013), no LES of a full engine has been published to date. This frontier has now been breached by Urbano *et al.* (2016*b*) who performed the first LES of a full rocket engine from the propellant injection domes, through the injectors and all the way to the exit nozzle.

The objective of the present work is to use this LES database to study high-frequency transverse CI. The configuration is first presented in Section 2 together with the operating conditions and the database of numerical simulations. Then Section 3 is devoted to the description of a mechanism that would explain the non-linear triggering of the transverse instability. Finally, in Section 4, the driving and damping terms of the acoustic energy equation are analyzed. Design guidelines are given for the development of laboratory-scale experiments that should exhibit self-excited transverse CI.

2. Configuration and LES database

The configuration is a reduced-scale rocket engine called BKD operated at DLR Lampoldshausen and consisting of a cylindrical combustion chamber, 8 cm in diameter, fed by 42 coaxial injectors and closed by a choked nozzle (Figure 1). The injection plate pattern

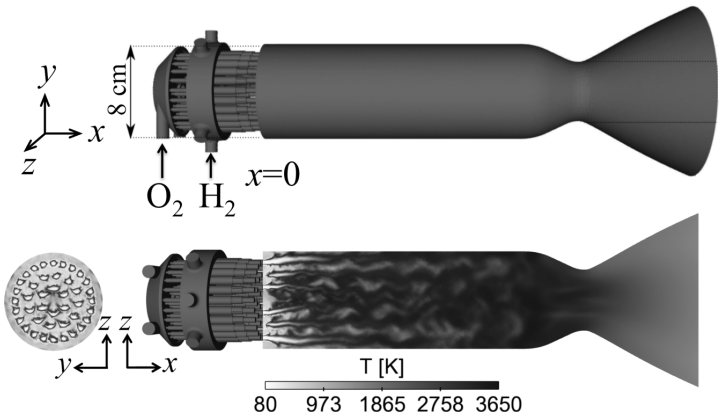

FIGURE 1. Overview of the computational domain for the BKD (top). Transverse (bottom left) and longitudinal (bottom right) cuts of instantaneous temperature field.

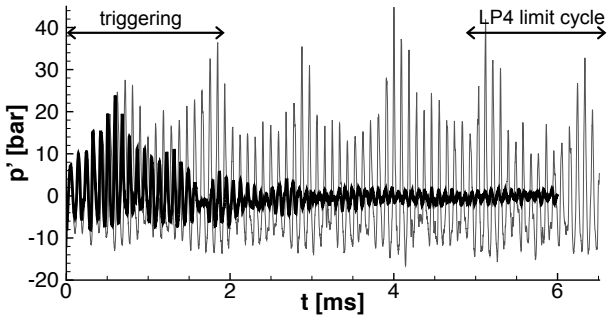

FIGURE 2. Temporal evolution of the pressure at the chamber wall, 5.5 mm downstream the injector plate. ——— stable operating point (LP1); – – – unstable operating point (LP4).

comprises three concentric rings of 6, 12 and 24 injectors, respectively. The propellants are oxygen and hydrogen, and the BKD is typically operated in the transcritical regime where liquid oxygen at subcritical temperature enters the chamber that is at supercritical pressure. For a detailed description of the apparatus, see Gröning *et al.* (2013, 2014).

The Large-Eddy Simulation of the BKD was performed by Urbano *et al.* (2016*b*) who showed that both stable (LP1) and unstable (LP4) operating conditions could be computed. The LES was linearly stable for both conditions, but with initial perturbation of magnitude beyond a certain threshold, LP4 would lock on a limit cycle CI. However, for LP1, the engine would return to stable operation for all perturbation levels tested (Urbano *et al.* 2016*b*). This behavior is referred to as a triggered instability and is illustrated in Figure 2 where the temporal evolution of the pressure at a probe on the chamber wall, five millimeters downstream the injector plate, is plotted.

As shown by Urbano *et al.* (2016*b*), the limit cycle CI is the combination of two frequencies corresponding, respectively, to the first transverse (Figure 3(a)) and the first radial (Figure 3(b)) modes of the combustion chamber. The fields of pressure fluctuations presented in Figure 3 were obtained via Dynamic Mode Decomposition (DMD). The DMD is an adequate tool for such cases where the pressure spectra are peaked and the corresponding modes are similar to those obtained via Fourier Transform (Urbano

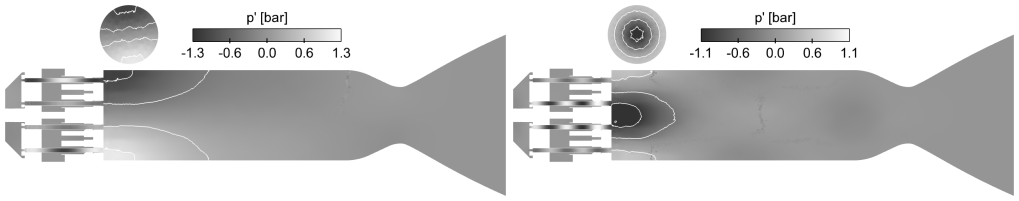

(a) 1T mode: $f_{1T} \sim 10.7$ kHz. (b) 1R mode: $f_{1R} \sim 21.4$ kHz.

FIGURE 3. Pressure fluctuation fields for the two main peaks obtained via DMD (Schmid 2010).

et al. 2016*b*). The 1R mode is almost exactly double the frequency of the 1T, but the drastic differences in their spatial structures indicate that the 1R is not simply a higher harmonic. It was also shown by Urbano *et al.* (2016*b*) that both modes can be found with a Helmholtz solver, an additional confirmation that they are not directly related. The analysis reported in this paper focuses on two specific periods of the time trace of Figure 2, namely

(*a*) From t=0 to t=2 ms: this is right after triggering induced by the pressure perturbation. The objective is to analyze how LP1 returns to stability while LP4 goes into a limit-cycle CI.

(*b*) From t=5 ms to t=6.5 ms: the limit cycle of LP4 is analyzed.

During these two time spans, the 3D fields of all variables of the simulation were saved at a sampling frequency of 100 kHz. This frequency corresponds to 200 solutions for the triggering analysis and 150 solutions for the limit cycle.

3. Analysis of triggering in the LES

The objective of this section is to propose a mechanism explaining the linear stability of LP4 and the switch to a limit cycle when sufficient initial perturbation is imposed. Consider the wave equation for linear acoustic pressure fluctuations, p', in a low-Mach reacting flow:

$$\frac{\partial^2 p'}{\partial t^2} - \rho_0 c_0^2 \vec{\nabla} \cdot \left(\frac{1}{\rho_0} \vec{\nabla} p' \right) = (\gamma - 1) \frac{\partial q'}{\partial t}, \tag{3.1}$$

where c_0 is the field of speed of sound, ρ_0 the time-averaged density field, γ the ratio of specific heat capacities and q' is the fluctuating heat release rate. It should first be pointed out that Eq. (3.1) is adequate for predicting transverse and radial modes in the BKD as there is no mean flow in these directions. It would, however, be inadequate for longitudinal modes because the mean Mach number in the chamber is not small (~ 0.3).

There are essentially two ways to explain triggering from Eq. (3.1):

(*a*) Flame driven: assuming that the unsteady flame response q' depends on the magnitude of the instability. There are numerous examples in the literature using the so-called Flame Describing Function (FDF) formalism, where triggering, mode-switching and limit-cycle amplitudes were predicted (Noiray *et al.* 2008; Silva *et al.* 2013).

(*b*) Field driven: assuming that the field of speed of sound c_0 is affected by the instability. To the authors' knowledge, this phenomenon has never been discussed.

In order to illustrate field-driven triggering, transverse cuts of speed of sound are presented at different times in Figure 4. Right after the initial perturbation (Figure 4(a)), long streaks of low c_0 corresponding to the elongated coaxial jet flames are visible throughout the chamber. With the establishment of the limit cycle (Figure 4(b)), the

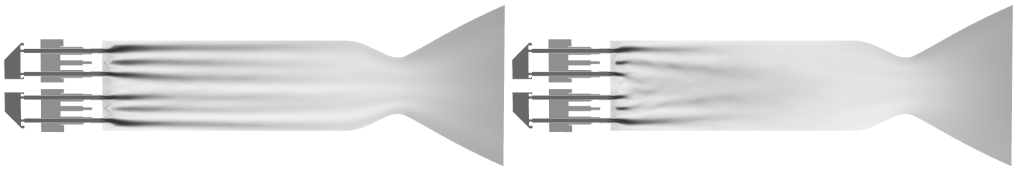

(a) $0 \leq t \leq 0.3$ ms. (b) $1.7 \leq t \leq 2$ ms

FIGURE 4. Sliding average of speed of sound field for LP4. Comparison of averages right after triggering and once the limit cycle has been established. Values of c_0 ranging from 240 m/s (black) to 2000 m/s (white).

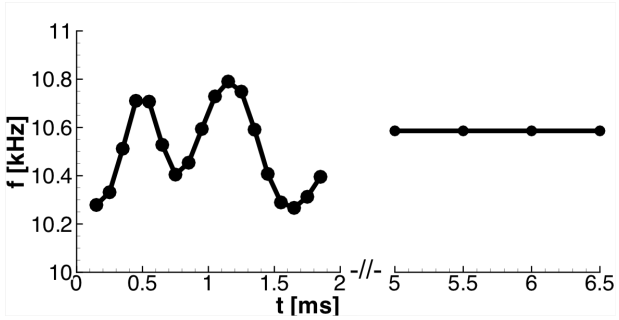

FIGURE 5. Temporal evolution of the 1T mode frequency of LP4 computed with a Helmholtz solver.

flames are shortened by the transverse velocity fluctuations so that the speed of sound is higher and more homogeneous after the first third of the chamber.

Solving Eq. (3.1) over the sliding average of the speed-of-sound field during the triggering allows the determination of the evolution of the frequency of the 1T mode. These values are compared to the frequency corresponding to the full-blown limit cycle of $t \in [5; 6.5]$ in Figure 5. Note that for the current analysis, the focus is on field-driven triggering so that the influence of the flame is neglected on purpose, by nulling the right-hand side of Eq. (3.1). This simplification should not affect the principle of the mechanism. At the onset of the triggering, before transverse velocity fluctuations affect the flame shapes, the frequency of the 1T mode is below 10.3 kHz. As the flames are shortened, the frequency oscillates, reaching values up to 10.8 kHz. This variation of about 5 % may be sufficient to drive the flame in and out of its stability margin. Because the limit cycle eventually establishes at 10.6 kHz, it is speculated that the 1T mode is initially stable at 10.3 kHz, and because of the significant amplitude of the initial perturbation, the flame shortening was able to move this frequency up. This mechanism should be verified in further work including the r.h.s of Eq. (3.1) through a model for the flame response.

As a side note, Eq. (3.1) is obtained with the additional assumptions that the fluid follows the perfect-gas law and that the mean pressure is constant. Despite the high pressure, these assumptions are valid in the high-temperature burnt gases. They are, however, crude in the regions where the cold reactants mix. A general version valid for any equation of state would be

$$\frac{\partial^2 p'}{\partial t^2} - \rho_0 c_0^2 \vec{\nabla} \cdot \left(\frac{1}{\rho_0} \vec{\nabla} p' \right) = \frac{\alpha c_0^2}{C_p} \frac{\partial q'}{\partial t}, \tag{3.2}$$

where α is the thermal expansion factor and C_p the constant pressure heat capacity. The influence of solving Eq. (3.2) instead of Eq. (3.1) is left for further studies.

4. Sources and dissipation of acoustic energy

In this section, the influence of the operating condition (LP4 versus LP1) on the stability is discussed by analyzing the source terms (driving and damping) for the acoustic energy. Following Brear *et al.* (2012), the acoustic balance equation, for an isentropic flow, at chemical equilibrium, neglecting viscous and diffusive terms, and considering a stationary base flow reads

$$\frac{\partial E_a}{\partial t} + F = R + D, \tag{4.1}$$

where E_a is the acoustic energy, F the acoustic fluxes, R the Rayleigh source term and D is the dissipation related to vorticity. These terms are defined as

$$E_a = \int_V \left(\frac{p'^2}{2\rho_0 c_0^2} + \frac{1}{2}\rho_0 \boldsymbol{u'}^2 + \rho' \boldsymbol{u_0} \boldsymbol{u'} \right) dV \tag{4.2}$$

$$F = \oint_S (p' + \rho_0 \boldsymbol{u}_0 \boldsymbol{u}') \left(\boldsymbol{u}' + \frac{\rho'}{\rho_0} \boldsymbol{u}_0 \right) dS \tag{4.3}$$

$$R = \int_V \left(\frac{\alpha_0}{\rho_0 C_{p0}} p' q' \right) dV \tag{4.4}$$

$$D = -\int_V m' . (\boldsymbol{\xi} \times \boldsymbol{u})' \, dV, \tag{4.5}$$

where $\boldsymbol{m'} = (\rho \boldsymbol{u})'$ and $\boldsymbol{\xi} = \boldsymbol{\nabla} \times \boldsymbol{u}$ is the vorticity. All variables are expressed as the sum of the stationary base flow (subcript 0) and a disturbance quantity (superscript '). For a generic field X, the decomposition is

$$X = X_0 + X'. \tag{4.6}$$

4.1. *Temporal analysis*

Figure 6 compares the evolutions of E_a, R and D for the first 2 ms after triggering. The initial pressure perturbation brings a sudden increase in the acoustic energy. However, for the stable case, E_a continuously decreases in time, as shown in Figure 6(a). On the other hand, for the unstable case, E_a oscillates, but is not damped. As a consequence, as previously observed in Figure 2, for the stable case LP1 the pressure oscillations are damped, whereas for the unstable case LP4, a limit cycle is reached. The evolution of the Rayleigh term is also reported in Figure 6(b) showing that the flame-acoustic coupling is strong for the unstable case: after a first burst around 0.7 ms, it decreases but keeps a mean value around 250 kW. By contrast, for the stable case, after the initial surge, R significantly decreases. Consequently, the flame response is a first reason for the different stability of LP1 and LP4. Now, the term D, shown in Figure 6(c), appears to be a low source term for the stable case, while being marginally negative on average, with strong oscillations for the unstable case. The contribution of D, representing the conversion between acoustics and vorticity, is qualitatively different between the two operating conditions: it is a marginally stabilizing term for the unstable case but a destabilizing contribution for the stable case. Obviously, with both R and D being positive for LP1, it is the fluxes F that make this case stable.

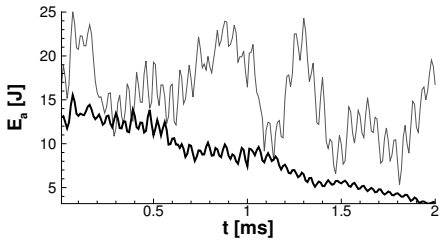

(a) Acoustic energy

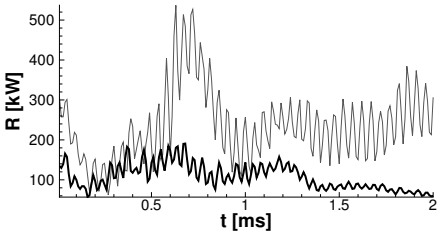

(b) Rayleigh term

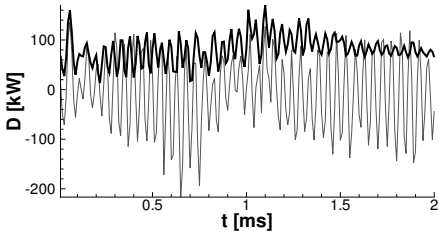

(c) Dissipation term

FIGURE 6. Acoustic energy, integrated Rayleigh and dissipation terms for the stable LP1 (dark line) and the unstable LP4 (light line) cases, over 2 ms.

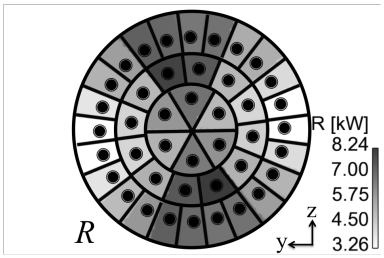

(a) R from Eq. (4.4).

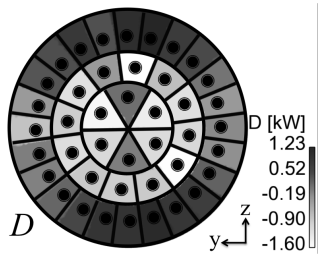

(b) D from Eq. (4.5).

FIGURE 7. Comparison of Rayleigh and dissipation terms. Averaging over volumes isolating individual flames and time average over the limit cycle ($5 \leq t \leq 6.5$ ms).

4.2. *Spatial analysis*

The question addressed in this section is the localization, during limit cycle, of the regions feeding and damping acoustic energy. The 150 3D solutions recorded between 5 and 6.5 ms are used for this purpose: the mean values of R and D are integrated over 42 volumes comprising single flames. The results are the maps of R and D shown in Figure 7.

Comparing the map of R with the shape of the 1T mode, flames located at pressure antinodes are the main contributors to the instability. Near the pressure nodal lines, the contribution is marginal. This feature is discussed by Urbano *et al.* (2016*a*). Similarly, the maps of D indicate that acoustic energy is dissipated around pressure nodes, whereas pressure antinodes show an average positive contributions from D.

4.3. *DMD analysis*

In this section, the use of DMD for the analysis of R and D is considered. From a more generic perspective, the application of DMD to non-linear combinations of variables is

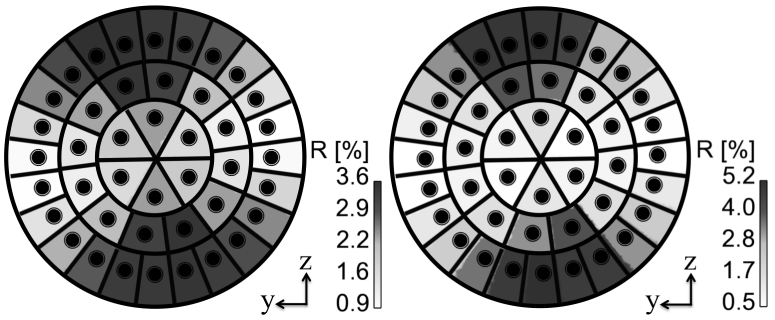

(a) DMD of Eq. (4.8) at $2 \times f_{1T}$. (b) $\langle R \rangle$ from Eq. (4.9).

FIGURE 8. Comparison of the Rayleigh maps obtained using the DMD of R and the reconstruction using the DMD of pressure and heat release rate fluctuations.

addressed. The problem is simplified by considering only the dominant frequency, f_{1T}, which corresponds to the 1T mode. The pressure and heat-release rate fluctuations may therefore be written as

$$p' = \bar{p}\ \cos(\omega t - \phi_p) \qquad q' = \bar{q}\ \cos(\omega t - \phi_q), \tag{4.7}$$

where $\bar{p}$ and ϕ_p (respectively, $\bar{q}$ and ϕ_q) are the modulus and phase of the DMD mode of the pressure (respectively, heat-release rate) at f_{1T} and $\omega = 2\pi f_{1T}$. Combining with Eq. (4.4) yields

$$R = \int_V \left[\frac{\alpha_0}{2\rho_0 C_{p0}} \bar{p}\bar{q} \left(\cos(2\omega t - (\phi_p + \phi_q)) + \cos(\phi_p - \phi_q) \right) \right] dV. \tag{4.8}$$

By choosing V as a volume enclosing a single flame (see Figure 7), Eq. (4.8) can be integrated during the limit cycle (i.e. from $t = 5$ ms to $t = 6.5$ ms). Because the limit cycle contains many periods of the oscillation, the first term of Eq. (4.8) vanishes and the time average is

$$\langle R \rangle = \int_V \frac{\alpha_0}{2\rho_0 C_{p0}} \bar{p}\bar{q} \cos(\phi_p - \phi_q) dV. \tag{4.9}$$

On the other hand, taking the DMD of Eq. (4.8) will yield a single mode at 2ω, which will have the same amplitude as $\langle R \rangle$ only without the factor $\cos(\phi_p - \phi_q)$. These two ways of analyzing the spatial distribution of R are compared in Figure 8. While it is clear that the DMD of R gives the same qualitative information as the true mean Rayleigh index $\langle R \rangle$, the missing $\cos(\phi_p - \phi_q)$ factor implies that the DMD of this non-linear quantity cannot be used for a quantitative estimation. Finally, because R is a quadratic quantity, the DMD mode of interest is at twice the frequency of the instability.

A similar analysis may be conducted for the dissipation term (Eq. (4.5)), although it is not reported here. Despite the fact that D appears to be a cubic combination of velocity fluctuations, after some algebra, only components at ω and $2 \times \omega$ remain.

5. Conclusions

In this paper, the LES of a 42 coaxial-injector rocket engine was analyzed with the objective of identifying the physical mechanism at play during a transverse combustion instability. Time-resolved series of 3D fields were processed with DMD in order to reconstruct pressure fluctuation fields. A mechanism that could explain the triggering of

the transverse CI was proposed, based on the modification of the field of speed-of-sound as the long coaxial diffusion flames are shortened by the transverse velocity fluctuations. The evolution of acoustic energy was studied, with special attention to terms resulting from the coupling between pressure and heat-release fluctuations (Rayleigh index) and also on the vorticity/acoustic velocity coupling (so-called dissipation term). It was found that the instability is driven mainly by the Rayleigh term at flames located at the pressure antinodes. Conversely, most of the damping stems from the flapping of the flames located at the velocity antinodes.

REFERENCES

Anderson, W. E. & Yang, V. 1995 *Liquid Rocket Engine Combustion Instability*, American Institute of Aeronautics and Astronautics.

Brear, M. J., Nicoud, F., Talei, M., Giauque, A. & Hawkes, E. R. 2012 Disturbance energy transport and sound production in gaseous combustion. *J. Fluid Mech.* **707**, 53–73.

Crocco, L. 1951 Aspects of combustion stability in liquid propellant rocket motors part i: fundamentals. Low frequency instability with monopropellants. *J. Am. Rocket Soc.* **21**, 163–178.

Crocco, L. 1952 Aspects of combustion stability in liquid propellant rocket motors part ii: low frequency instability with bipropellants. high frequency instability. *J. Am. Rocket Soc.* **22**, 7–16.

Crocco, L., Harrje, D. T. & Reardon, F. H. 1962 Transverse combustion instability in liquid propellant rocket motors. *ARS J.* **32**, 366–373.

Culick, F. E. C. 1988 Combustion instabilities in liquid-fuelled propulsion systems. In *AGARD 72B PEP Meeting*, pp. 1–74.

Gröning, S., Suslov, D., Hardi, J. & Oschwald, M. 2014 Influence of hydrogen temperature on the acoustics of a rocket engine combustion chamber operated with LOX/H2 at representative conditions. In *Space Propulsion*. Cologne: Association aéronautique et astronautique de France (3AF).

Gröning, S., Suslov, D., Oschwald, M. & Sattelmayer, T. 2013 Stability behaviour of a cylindrical rocket engine combustion chamber operated with liquid hydrogen and liquid oxygen. In *5th European Conference for Aeronautics and Space Sciences*. Munich.

Hakim, L., Ruiz, A., Schmitt, T., Boileau, M., Staffelbach, G., Ducruix, S., Cuenot, B. & Candel, S. 2015 Large eddy simulations of multiple transcritical coaxial flames submitted to a high-frequency transverse acoustic modulation. *Proc. Combust. Inst.* **35**, 1461–1468.

Hardi, J. S., Beinke, S. K., Oschwald, M. & Dally, B. B. 2014 Coupling of cryogenic oxygen hydrogen flames to longitudinal and transverse acoustic instabilities. *J. Propul. Power* **30**, 991–1004.

Harrje, D. T. & Reardon, F. H. 1972 *Liquid Propellant Rocket Combustion Instability*, NASA Tech. Rep. #NASA-SP-194.

Lieuwen, T. C. 2012 *Unsteady Combustor Physics*. Cambridge University Press.

Lubarsky, E., Hadjipanayis, M., Shcherbik, D., Bibik, O. & Zinn, B. 2008 Control of tangential instability by asymmetric baffle. In *46th AIAA Aerospace Sciences Meeting and Exhibit*, Reno, Nevada.

Méry, Y., Hakim, L., Scouflaire, P., Vingert, L., Ducruix, S. & Candel, S. 2013 Experimental investigation of cryogenic flame dynamics under transverse acoustic modulations. *C. R. Mecanique* **341**, 100–109.

Noiray, N., Durox, D., Schuller, T. & Candel, S. 2008 A unified framework for nonlinear combustion instability analysis based on the flame describing function. *J. Fluid Mech.* **615**, 139.

Oefelein, J. C. & Yang, V. 1993 Comprehensive review of liquid-propellant combustion instabilities in F-1 engines. *J. Propul. Power* **9** (5), 657–677.

Poinsot, T. & Veynante, D. 2011 *Theoretical And Numerical Combustion*, 3rd ed. www.cerfacs.fr/elearning.

Popov, P. P., Sideris, A. & Sirignano, W. a. 2014 Stochastic modelling of transverse wave instability in a liquid-propellant rocket engine. *J. Fluid Mech.* **745**, 62–91.

Rayleigh, J. W. S. 1878 The explanation or certain acoustic phenomena. *Nature* **18**, 319.

Sattelmayer, T., Schmid, M. & Schulze, M. 2015 Interaction of Combustion with transverse velocity fluctuations in liquid rocket engines. *J. Propul. Power* **31**, 1137–1147.

Schmid, P. 2010 Dynamic mode decomposition of numerical and experimental data. *J. Fluid Mech.* **656**, 5–28.

Searby, G., Nicole, A., Habiballah, M. & Laroche, E. 2008 Prediction of the Efficiency of Acoustic Damping Cavities. *J. Propul. Power* **24**, 516–523.

Silva, C. F., Nicoud, F., Schuller, T., Durox, D. & Candel, S. 2013 Combining a Helmholtz solver with the flame describing function to assess combustion instability in a premixed swirled combustor. *Combust. Flame* **160**, 1743–1754.

Sirignano, W. A. & Popov, P. P. 2013 Two-dimensional model for liquid-rocket transverse combustion instability. *AIAA J.* **51**, 2919–2934.

Urbano, A., Douasbin, Q., Selle, L., Staffelbach, G., Cuenot, B., Schmitt, T., Ducruix, S. & Candel, S. 2016*a* Study of flame response to transverse acoustic modes from the les of a 42-injector rocket engine. *Proc. Combust. Inst.* (In Press).

Urbano, A., Selle, L., Staffelbach, G., Cuenot, B., Schmitt, T., Ducruix, S. & Candel, S. 2016*b* Exploration of combustion instability triggering using large eddy simulation of a multiple injector liquid rocket engine. *Combust. Flame* **169**, 129–140.

You, D., Ku, D. D. & Yang, V. 2013 Acoustic waves in baffled combustion chamber with radial and circumferential blades. *J. Propul. Power* **29**, 1–15.